# The petrophysical basis for shallow-water flow prediction using multicomponent seismic data

*Alan R. Huffman, Conoco, Houston, Texas, U.S.*
*John P. Castagna, University of Oklahoma, Norman, U.S.*

Physical properties of shallow-water flow (SWF) sands differ from most reservoir and seal rocks studied for petroleum purposes. These materials exist near the transition zone between rocks and sediments. Our investigations, the subject of this article, suggest that physical properties of SWF sands are amenable to a prediction methodology that uses high-resolution multicomponent seismic data.

SWF sands are a primary hazard to deepwater drilling operations in the Gulf of Mexico. They have the potential to result in well failures and significant discharges of subsurface fluids into the ocean. However, at present, most operators make only a modest attempt to identify SWF before drilling. They drill through these hazards and mitigate any resulting damage at significant expense if one is encountered. This is not rare. According to a report from Fugro Geoservices, approximately 70% of all deepwater wells have experienced SWF.

A method for predrill delineation of sands that are close to failure, and thus likely to exhibit SWF, would be advantageous in selecting optimal drilling locations and in developing cost-effective well plans. The current method of identifying SWF involves predrill hazard studies utilizing conventional and high-resolution seismic data to identify zones that might produce SWF. However, the high incidence of SWF mitigation events in deepwater wells shows that existing techniques do not provide adequate resolution or accuracy.

At present, no robust seismic method exists for accurately identifying and characterizing SWF. Operators do not have the option to avoid the hazard instead of mitigating the problem after it has started. A new method is required that will permit operators to identify the hazard before the well is drilled.

Using seismic data for accurate understanding of the physical properties and deformational behavior of SWF sands is essential to characterization, prediction, and interpretation of these stratigraphic units. To date, very few core and log formation evaluation measurements have been taken in these shallow intervals because they are not of economic interest.

**Physical conditions of SWF formations.** SWF sands have been observed in water depths 1500-7000 ft beneath the seabed and 4000 ft below the mud line. At these depths of burial, materials are virtually unconsolidated and have very high porosities and very low effective stresses. The range of confining and effective stresses for these sands can be estimated from first principles to be, respectively, 700-6500 psi and 0-1000 psi. To put this in perspective, it is valuable to compare stress conditions in a shallow-water and a deepwater case (Figure 1). In both, effective stress on the formation at the mud line is zero. It increases with a gradient of about 0.535psi/ft if hydrologic communication is maintained with the ocean water column. In shallow water, effective stress becomes nonzero 500 ft below sea level where the total overburden stress is relatively small. At a water depth of 4000 ft, however, overburden stress is much larger due to the higher water column. However, as long as pore fluids are in pressure communication, pore pressure will increase an equal amount. Thus, effective stress remains unchanged between shallow and deepwater at the same depth below mud line. In this example case, it is possible that an SWF zone could be 6000 ft below mean sea level and 2000 ft below mud line and exist at a confining stress of 3100 psi and an effective stress of about 1100 psi. This compares to a shallow-water case (water depth of 500

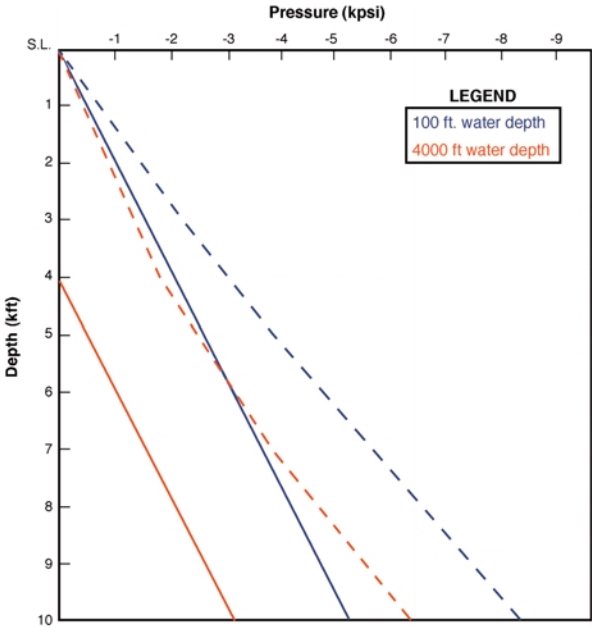


**Figure 1. Examples of confining stress (dashed curves) and effective stress (solid curves) from shallow water (blue curves) and deep water (red curves) showing the contrast in loading conditions. Note that the difference between the red curves at depths of 4000 and 7000 ft, which represents the pore pressure, is much larger than the difference between the blue curves at the same depth.**

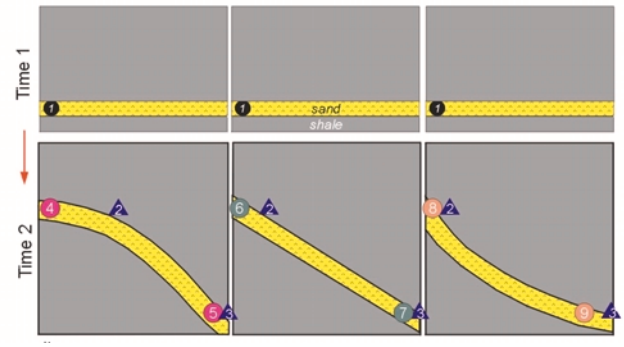


**Figure 2. Model of sand deposited on a flat surface and then positioned structurally to create a hyperpressured reservoir. At time 1, the sand is in equilibrium with all pressures equal. At time 2, sand pressures are different with respect to each other and with respect to the pressures in the adjacent shales and are affected by the type of structure. (From Stump et al.)**

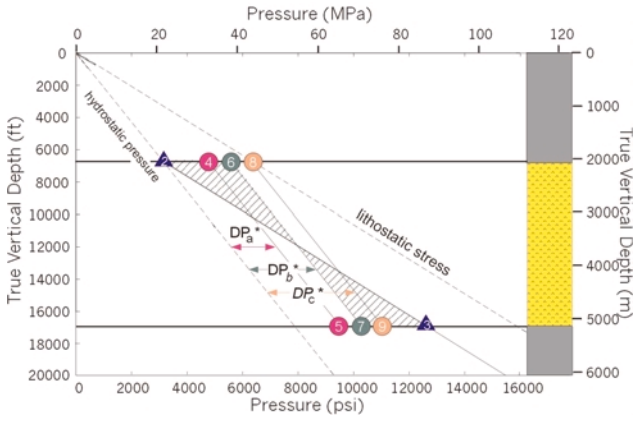


**Figure 3. Pressure diagram showing relationship between structurally hyperpressured sand in Figure 2 and the surrounding shales. Numbers correspond to numbers defining structural position of each sand in Figure 2. Numbers 4, 6, and 8 represent pressure at the top of the sand body. Numbers 5, 7, and 9 represent pressures at the bottom of the sand. Numbers 2 and 3 are pressures at the top and bottom of the shale. The centroid of each sand is the point at which reservoir pressure intersects shale pressure. (From Stump et al.)**

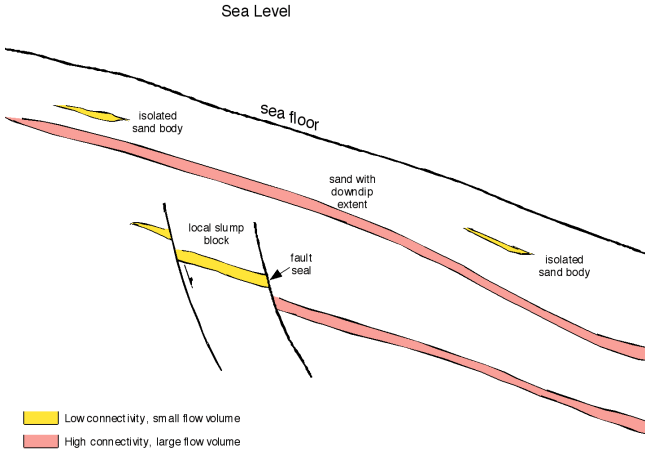


**Figure 4. Types of shallow-flowing sands characterized by their hydrologic continuity and ability to produce a given volume of fluid. Note the large volume of water that can be produced by sands that have large downdip extents and structural hyperpressuring (red) versus those with small extent (yellow).**

ft) in which the confining stress is 4750 psi and the effective stress is 3100 psi. The pore pressures that equate to these two cases are 2000 psi for deep water and 1650 psi for shallow water, or a difference of 350 psi at the same depth relative to sea level. Thus, not only are sediments in the deepwater case less compacted, but they are at relatively higher pore pressures for the same depth below sea level.

In addition to the change in compaction state for deepwater sediments, the severity of SWF may be exacerbated by the presence of structural hyperpressuring, also known as the centroid effect (Traugott and Heppard, 1994). The concept of structural hyperpressuring suggests that a sand body on a structure or slope will develop a pressure gradient that is hydrostatic, even though the gradient in the surrounding sediments is nonhydrostatic (Figures 2 and 3). This effect produces a condition in which the updip limb of a sand body with large areal extent may have much

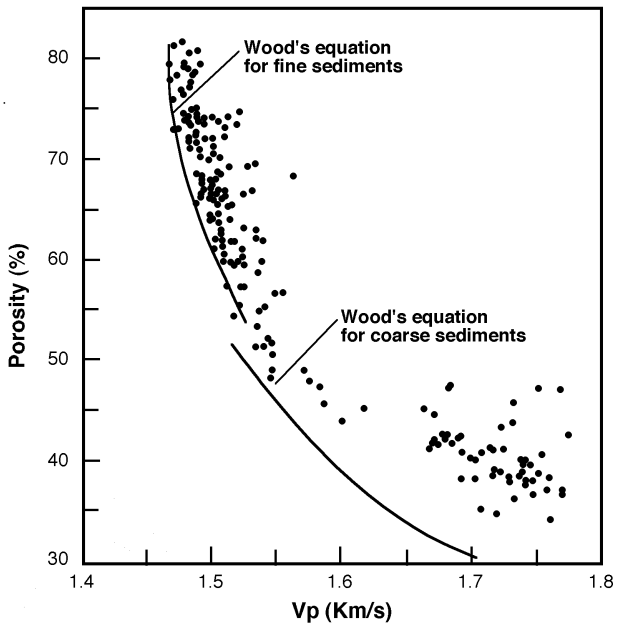


**Figure 5. Porosity velocity relationships observed in marine sediments. Differences between the measurements and the curves for Wood's equation are probably due to development of frame rigidity. (After Smith.)**

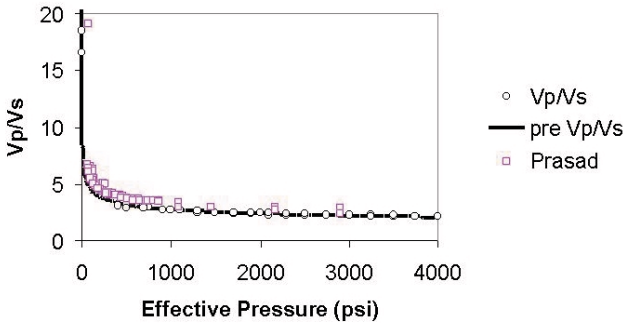


**Figure 6. Pulse transmission measurements on brine-saturated sand packs. Open circles are our data which are fit by a power-law empirical relation, as described in the text (solid line). Open squares are measurements from Prasad.**

higher pore pressures than the surrounding shales (they can even approach the fracture gradient). The character of the structure (e.g., synclinal versus anticlinal) also determines the reservoir pressure to some extent (Figure 3). For the shallow burial conditions in which SWF occur, the amount of structural hyperpressuring required to cause a seal failure is not large. Hence, it is easy to picture a situation (Figure 4) in which a sand is deposited on the slope with a large downdip extent and then buried under a finite amount of overburden, producing a structurally hyperpressured reservoir that will result in SWF when penetrated.

**Petrophysical properties.** To understand the petrophysical properties of SWF sands, one must consider their deposition and burial. Sands and shales are deposited on the seabed in a form that resembles a slurry more than a rock. Smith (1974) characterized the behavior of these fine- and coarse-grained sediments using Wood's equation for suspensions (Figure 5). As materials are buried, they begin to deviate from the Wood's equation and become load-bear-

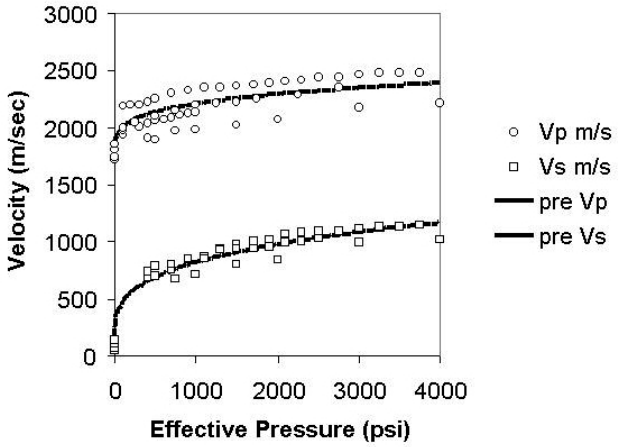


**Figure 7. Pulse transmission water-saturated $V_P$ (open circles) and $V_S$ (open squares) measurements from this study, including the data of Bell (1979) and Domenico (1977). Solid lines are power-law fits to the $V_P$ and $V_S$ data, as described in the text.**

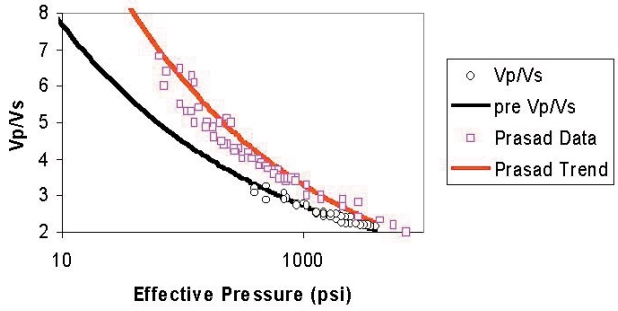


**Figure 8. $V_P/V_S$ ratio plotted against effective pressure on a logarithmic scale for pressures between 10 and 10 000 psi and $V_P/V_S$ less than 8. Open circles are measurements from this study on clean brine-saturated sands, and open squares are measurements by Prasad. Solid line is predicted $V_P/V_S$ from power-law fit to our measurements. Solid red line is Prasad's reported empirical fit.**

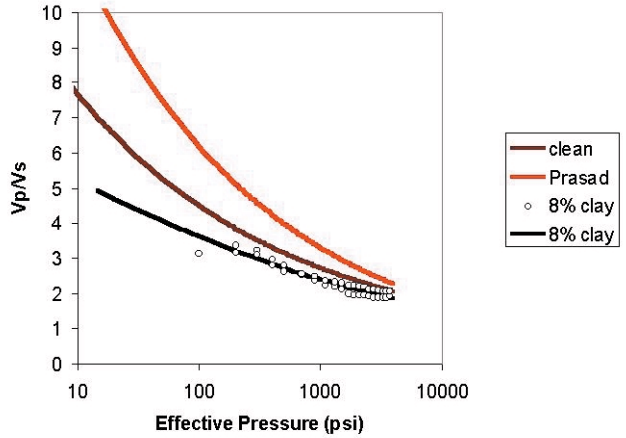


**Figure 9. $V_P/V_S$ plotted against effective stress for brine-saturated sand packs containing 8% clay by weight (open circles) and power-law empirical fit. Brown line is the clean sand trend from Figure 8. Red line is Prasad's reported trend.**

ing materials with a granular frame that develops rigidity. The porosity point at which sediments begin to behave like load-bearing framework solids was termed the "critical porosity" by Amos Nur. This change in behavior is an important transition because it signals the point at which effective stress becomes nonzero. As effective stress increases, compaction causes porosity to decrease and the material becomes more rocklike in its behavior. However, the slower rate of increase in effective stress in deepwater conditions also causes the rate of compaction to decrease, causing these materials to have a relatively higher porosity than a shallow-water material at the same depth below sea level.

Evaluation of the physical properties pertinent for predrill seismic characterization of SWF must include compressional and shear velocities, attenuation and densities of the materials, and the strength of the sand framework under dynamic loading. Basic understanding of these properties can be estimated from first principles of compaction theory for sediments and soils, and from the literature on velocity-effective stress relationships in clastic sediments. If we consider the range of confining and effective stresses under which SWF sands exist, it is recognized that these materials exist in the transition zone between Wood's equation behavior for slurries and porous load-bearing granular materials that can be modeled using Biot theory. At these conditions, the formation should show modest changes in compressional velocity with the observed pore-pressure changes. In contrast, small changes in pore pressure will cause large changes in shear-wave velocity as the material moves very close to the critical porosity which results in the rigidity, or shear strength, of the material rapidly approaching zero. The combination of these two predictions suggests that the $V_P/V_S$ ratio of these sands may change dramatically under small load changes (Figure 6). The equations of Castagna et al. (1993) suggest that below a certain effective stress, there is a rapid increase in the $V_P/V_S$ ratio (which is directly related to Poisson's ratio). It is reasonable to assume that this is accompanied by a rapid increase in shear-wave attenuation with very small decreases in effective stress. This occurs because rock rigidity is approaching zero (i.e., the sediment is becoming more like a liquid). At higher effective stresses, the rock frame is more rigid and the sediment behaves more like a solid. The region of rapid rigidity loss is a likely candidate for SWF. The loss of rigidity may also be tied back to the strength of the materials and their resistance to liquefaction and formation collapse. Poisson's ratio, the modulus of rigidity, and shear-wave quality factor (Q or attenuation) should be highly anomalous for sands close to failure and prone to SWF.

To confirm the above postulates, measurements of compressional- and shear-wave velocities were performed under a range of confining and pore pressure conditions appropriate for SWF problems—porosities of 32-50%, 0-8% shale, and a range of frequencies using conventional ultrasonic pulse transmission techniques. These measurements were performed at the IC3 facility (the former BP Amoco rock-physics lab known as the Integrated Core Characterization Center) at the University of Oklahoma in Tulsa. The data set was completed by measuring the dry velocities on a sand pack and then backfilling with brine to measure water-saturated properties. Effective stress varied from 3750 psi to 200 psi in dry samples and down to 400 psi in saturated samples. Shear-wave measurements were stopped at these two stresses, respectively, due to loss of coupling of the transducers to the sample and/or

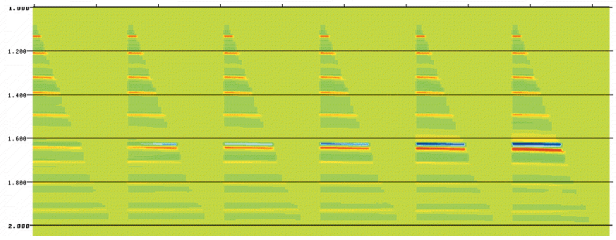

**Figure 10. Seismic gathers for *P*-wave reflection events from model showing change in reflectivity with effective stress. Left model is a reference shale layer. Models 2-6 represent decreasing effective stress from 3750 psi down to 100 psi.**

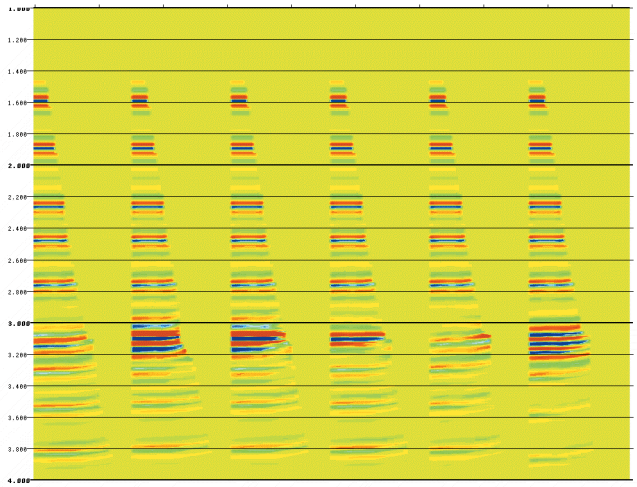

**Figure 11. Seismic gathers for mode-converted *S*-wave reflection (*PS*) events from model showing change in reflectivity with effective stress. Left model is a reference shale layer. Models 2-6 represent decreasing effective stress from 3750 psi down to 100 psi. Note large change in polarity and reflection strength between gathers 4 and 6.**

increased shear-wave attenuation; either resulted in inability to detect the transmitted shear wave.

Figure 7 shows a compilation water-saturated $V_P$ and $V_S$ measurements from this study, with the data of Bell (1979) and Domenico (1977) added. The velocities are readily fit by power-law equations of the form

$$V = a + b\,P^c$$

where P is the effective pressure. The constant $a$ is constrained by Wood's equation at zero effective stress for *P*-wave velocities and is taken to be zero for shear-wave velocities in clean sands. The empirical coefficients $b$ and $c$ are then obtained by curve fitting the data. We find for the clean sands in Figure 7 (velocity is m/s and pressure in bars)

| | | | |
|---|---|---|---|
| $V_P$: | $a = 1700$, | $b = 200$, | $c = .22$ |
| $V_S$: | $a = 0$, | $b = 270$, | $c = .26$ |

It is obvious by inspection of Figure 7 that the data can only be approximately fit by equations of this form because the coefficients will vary with porosity and composition. However, when taking the ratio of $V_P$ to $V_S$, the scatter is much reduced (Figure 8) and a remarkably good fit results. The data of Prasad (in press and also shown in Figure 8) are in general agreement with the $V_P/V_S$ trend but higher $V_P/V_S$ ratios (we suspect this is due to higher porosities in Prasad's samples). Clearly, the spread in the data suggests that additional calibration of $V_P/V_S$ trends will be needed.

We find a similar a power-law pressure dependence for sand packs that have 8% clay by weight. For these clay-rich sand packs, we find

| | | | |
|---|---|---|---|
| $V_P$: | $a = 1640$, | $b = 180$, | $c = .26$ |
| $V_S$: | $a = 160$, | $b = 210$, | $c = .30$ |

The resulting $V_P/V_S$ trend (Figure 9) exhibits lower $V_P/V_S$ than the clean sand trend from this study and Prasad's trend. These low $V_P/V_S$ ratios may indicate that small amounts of clay act to bind the loose sand grains, thereby decreasing $V_P/V_S$ at a given pressure.

**Models for SWF seismic response.** The laboratory measurements of compressional- and shear-wave velocities associated with pressure changes in the sands were used to generate a series of seismic model responses. Models comprised multiple layers of shale with montonically increasing velocity and density and with an imbedded sand layer representing the SWF reservoir unit.

The model results suggest that the large changes predicted in $V_S$ and $V_P/V_S$ ratio will result in significant changes in the AVO response of the SWF sand units. The *P*-wave gathers (Figure 10) show a modest change in reflectivity and a significant change in the reservoir's AVO response as a function of effective stress. Likewise, the mode-converted *S*-wave gathers, or *PS* events (Figure 11), show a dramatic change in reflectivity and a change in polarity as a function of effective stress. The *PS* reflection gathers also show significant attenuation on the low effective stress models not present on the higher effective stress models. Furthermore, the large changes in attenuation exhibited by these sands will also cause significant frequency loss on seismic data. The seismic responses from these models indicate that high-resolution AVO and inversion methods should be able to resolve the changes in pressure and failure state that are related to the SWF problem. Analysis of the attenuation properties also suggests that changes in attenuation should be observed below sands that are abnormally pressured and prone to SWF, as evidenced by the loss of reflectivity at low effective stresses in Figure 11. It is also highly likely that given multicomponent seismic data, Poisson's ratio, modulus of rigidity, and shear-wave quality factor can be extracted with greater resolution and accuracy than from conventional seismic data. Attenuation should be detectable, particularly on multicomponent data, by analyzing the *P*-wave reflections from the SWF zone and mode-converted shear-wave reflections from SWF intervals and below them. Attenuation of both *P*- and *S*-reflections that have traveled through the SWF zone should be significant and should allow these zones to be mapped.

To determine whether real multicomponent data can resolve changes in physical properties associated with SWF conditions, we worked in conjunction with PGS Reservoir to evaluate the value of these data for shallow hazard analysis. Various sites were selected from the Gulf of Mexico (GOM), where PGS has acquired 2-D multicomponent ocean-bottom cable data (OBC). A proprietary multicomponent $V_P/V_S$ inversion method was applied to these data. Results suggest that the variations in velocity and impedance resulting from SWF sand bodies will be detectable on seismic data (Figure 12). In particular, it appears that mode-converted shear-wave data are particularly useful in obtaining a high-resolution estimate of $V_P/V_S$.

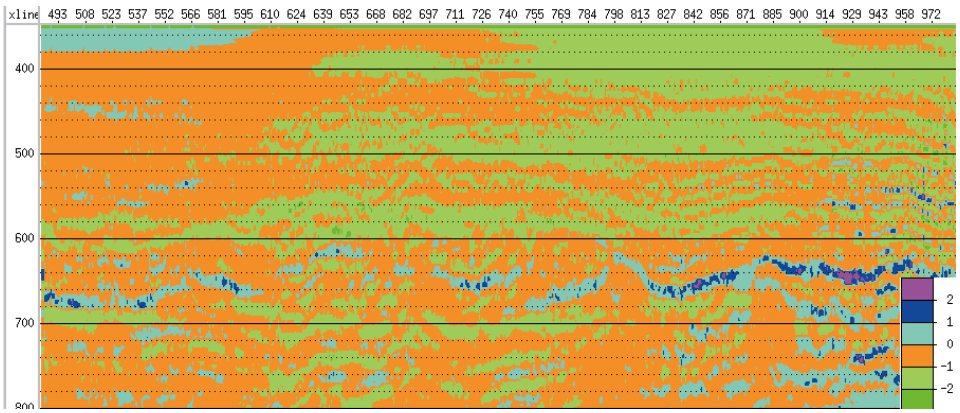


**Figure 12. Multicomponent seismic inversion for a deep-water Gulf of Mexico data set showing deviation in $V_P/V_S$ ratio from the mud-rock trend. Purple and blue are zones with abnormally high $V_P/V_S$ relative to expectation, possibly indicating sand bodies close to failure. Vertical axis is *PP* time relative to mud line.**

We also investigated the use of conventional AVO analysis of shallow reflections. Such analysis is problematic for OBC data because the unusual geometry is not well suited for AVO analysis of shallow events. However, conventional AVO analysis was performed to see if anomalous behavior could be observed empirically. Figure 13 shows an apparent high Poisson's ratio anomaly in the vicinity of a well exhibiting a shallow-water flow.

**Mechanical failure.** At very low effective stresses, physical conditions in these SWF sands are such that they are close to critical porosity with porosities from 38% to 50%, depending on the sorting and shaliness of the specific stratigraphic unit. The high porosities and uncemented, unconsolidated nature of these sands plus the very low effective stresses also suggest that they should have very low failure strengths and may exist in a state of incipient failure that allows them to flow into a well bore when penetrated by the drill bit. SWF sands often are abnormally pressured up to 200 psi above the surrounding sediments, which may increase the mechanical instability that leads to significant flows. In a relative sense, the actual pore pressure difference in these sands is very small, often less than 100 psi. However, such small changes in pressure at these shallow depths of burial can lead to significant water flows that can cause formation collapse and massive sanding into a well. The unconsolidated state of these sediments also provides sufficient formation porosity such that the volume of producible water can be quite large. When an SWF sand has an extensive downdip extent, the volume of producible water and the hydrostatic support available to maintain the flow for long periods of time can be severe.

A major question regarding SWF is the cause of failure. At present, there are two likely possibilities.

First, it is possible that these materials are already in an incipient state of failure and that drilling simply initiates the flow by dynamic loading of the sediments at the well-bore interface. The analog for this type of failure is well known in earthquake literature and is called liquefaction. Liquefiable materials documented from earthquake studies (Richart et al., 1970) tend to be high porosity and of a coarse granular nature, very similar to SWF sands. These failures are caused by the rearrangement of grains due to dynamic loading that causes the local pore pressure to increase dramatically as the material attempts to compact under the loading. Such materials have been documented to flow to the surface and vent spectacularly, as has been observed in some SWF case studies.

Second, it is possible that these materials are so cohesionless that the mere flow of formation water into the well bore causes the sand to flow as well, and that the sustained flow of formation water eventually destabilizes the entire formation and results in a total collapse of the SWF interval. Effectively, this is a type of catastrophic sanding problem.

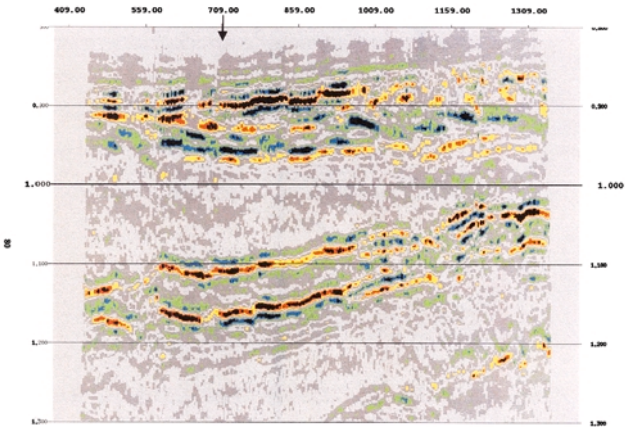


**Figure 13. AVO analysis showing an abnormally high Poisson's ratio anomaly at about .9 s in the vicinity of a well exhibiting shallow-water flow. Red indicates positive Poisson's ratio anomalies, and blue indicates negative anomalies. The arrow is the well location.**

The difference between these two failure modes is significant. Catastrophic sanding can likely be mitigated by changes in drilling fluid pressure and properties but liquefaction must be mitigated by decreasing the dynamic loading induced by the drilling operation so that the formation does not "feel" the drill bit passing through it. More direct measurements of SWF zones while drilling are needed to determine which failure mode is occurring. It is possible that both failure modes are present, but the data available to date are insufficient to distinguish between them.

**Conclusions.** Physical properties of SWF sands differ from most reservoir and seal rocks studied for petroleum purposes. These materials exist near the transition between rocks and sediments, and the results of this study suggest that the physical properties of SWF sands are amenable to a prediction methology that includes inversion, seismic attributes, and attenuation analysis. Combining these methods with high-resolution multicomponent seismic acquisition and processing should help avoid these costly hazards and prevent costly well failures in the future. If you are interested in learning more about the PGS/ERCH Shallow Water Flow Project, contact Gene Sparkman at 1-281-363-7936 or *sparkman@erch.harc.edu.*

*(Continued on p. 1052)*

*(Huffman, from p. 1035)*

**Suggested reading.** "Rock physics—the link between rock properties and AVO response" by Castagna et al. (in *Offset-Dependent Reflectivity—Theory and Practice of AVO Analysis*, SEG, 1993). "Elasticity of high-porosity sandstones: Theory for two North Sea data sets" by Dvorkin and Nur (GEOPHYSICS, 1996). "Pressure differences between overpressured sands and bounding shales of the Eugene Island 330 Field (Offshore Louisiana, USA) with implications for fluid flow induced by sediment loading" by Stump et al. (in *Overpressures in Petroleum Exploration*, Memoire 22, Elf EP Editions, 1998). "Percolation of electrical and elastic properties of granular materials at the transition from a suspension to a loose packing" by Marion and Nur (*Physica A*, 1989). "Compressional velocity and porosity in sand-clay mixtures" by Marion et al. (GEOPHYSICS, 1992). "Critical porosity: A key to relating physical properties to porosity in rocks" by Nur et al. (*TLE*, 1998). *Vibrations of Soils and Foundations* by Richart et al. (Prentice Hall, 1970). "Acoustic and mechanical loading of marine sediments" by Smith (in *Physics of Sound in Marine Sediments*, Plenum Press, 1974). "Prediction of pore pressures before and after drilling—Taking the risk out of drilling overpressured prospects" by Traugott and Heppard (in *Abnormal Pressures in Hydrocarbon Environments*, AAPG, 1994). **E**

*Acknowledgments: Laboratory measurements were made by Carl Sondergeld and Bruce Spears at the University of Oklahoma. Seismic modeling was performed by Surinder Sahai at Conoco. Sahai and Santi Randazzo (PGS) processed the seismic data. Multicomponent seismic inversion was conducted by Carlos Moreno at the University of Oklahoma. Many thanks to Allen Bertagne of PGS Reservoir and Gene Sparkman and Roger Entralgo of ERCH for coordinating efforts. Thanks to Conoco and PGS Reservoir for permission to publish this paper.*

*Corresponding author: Alan.R.Huffman@usa.conoco.com*